Accepted Manuscript

Title: Mathematical modelling and validation of CO_2 mass transfer in a membrane contactor using ionic liquids for pre-combustion CO_2 capture

Authors: Muhammad Usman, Zhongde Dai, Magne Hillestad, Liyuan Deng

Please cite this article as: Usman, Muhammad, Dai, Zhongde, Hillestad, Magne, Deng, Liyuan, Mathematical modelling and validation of CO2 mass transfer in a membrane contactor using ionic liquids for pre-combustion CO2 capture.Chemical Engineering Research and Design http://dx.doi.org/10.1016/j.cherd.2017.05.026

This is a PDF file of an unedited manuscript that has been accepted for publication. As a service to our customers we are providing this early version of the manuscript. The manuscript will undergo copyediting, typesetting, and review of the resulting proof before it is published in its final form. Please note that during the production process errors may be discovered which could affect the content, and all legal disclaimers that apply to the journal pertain.

Mathematical modelling and validation of CO_2 mass transfer in a membrane contactor using ionic liquids for pre-combustion CO_2 capture

Muhammad Usman, Zhongde Dai, Magne Hillestad*, Liyuan Deng*

Norwegian University of Science and Technology (NTNU), Trondheim 7491, Norway

* deng@nt.ntnu.no; magne.hillestad@ntnu.no

1. Highlights

- 1D-model of membrane contactor based on ionic liquid for pre-combustion CO_2 capture was developed.
- Both wetted and non-wetted modes of operation of membrane were considered for model development.
- The model was validated with experimental data and showed AARD value lower than 8%.
- A new mass transfer resistance term was added to reflect the non-flat concentration profile in the liquid phase.
- Separation performance of membrane contactor were systematically investigated.

Abstract

Mass transfer and mathematical modelling of CO_2 absorption in a tubular membrane contactor using 1‑Butyl-3-methylimidazolium Tricyanomethanide ([Bmim][TCM]) for pre-combustion CO_2 capture has been studied in this work. A 1D-model was developed based on resistance in series model and CO_2 material balance. The developed model was validated with the experimental data, and good agreement was observed between the simulated and experimental results. A new mass transfer resistance term is added to reflect the non-flat concentration profile in the liquid phase. Simulation results indicate that the liquid phase resistance contributes 67 % and 44 % to the total mass transfer resistance for non-wetted and wetted modes of membrane, respectively. The resistance that occurred due to considering transport in liquid phase

contributes 31 and 20% for non-wetted and wetted modes of membrane contactor, respectively. CO_2 flux along the axial length of membrane contactor was modeled, giving the maxima at the gas outlet. The influences of operational constraints including liquid/gas flow rates, operation pressure/ temperature, length of membrane contactor, and CO_2 concentration in feed gas were also inspected.

Keywords: CO_2 capture; Pre-combustion; Ionic liquid; Mass transfer study; Membrane contactor; modelling

Nomenclature

A_m	Membrane area (m^2)
C_{IL}	Concentration of BmimTCM (mol.m^{-3})
C_{co2}^{G}	Concentration of CO_2 in gas phase (mol.m^{-3})
C_{co2}^{L}	Concentration of CO_2 in liquid phase (mol.m^{-3})
$C_{co2}^{i,g}$	Concentration of CO_2 at the gas side on interface(mol.m^{-3})
$C_{co2}^{i,l}$	Concentration of CO_2 at the liquid side on interface(mol.m^{-3})
C_{co2}^{out}	Concentration of CO_2 at the gas outlet (-)
d_h	Hydraulic diameter of membrane (m)
d_i	Inner diameter of membrane (m)
d_o	Outer diameter of membrane (m)
$D_{co2,m}$	Effective diffusivity of CO_2 (m^2.s^{-1})
$D_{g,co2}$	Diffusivity of CO_2 in gas phase(m^2.s^{-1})
$D_{l,co2}$	Diffusivity of CO_2 in liquid phase(m^2.s^{-1})
F_G	Molar gas flow rate (mol.m^2.s^{-1})
F_L	Molar liquid flow rate (mol.m^2.s^{-1})
GFR	Gas volumetric flow rate (m^3.hr^{-1})
H_{co2}	Henry's constant of CO_2 (MPa)
k_g	Gas side mass transfer coefficient (m.s^{-1})
k_l	Liquid side mass transfer coefficient (m.s^{-1})
k_m	Membrane mass transfer coefficient (m.s^{-1})
K_{ov}	Overall mass transfer coefficient (m.s^{-1})
L	Length of membrane contactor (m)
LFR	Liquid volumetric flow rate (m^3.hr^{-1})
m	Dimensionless Henry's constant (-)
N_{CO2}	CO_2 absorption flux (mol.m^2.s^{-1})

n_{co2}^{in}	Mole fraction of CO_2 at the gas inlet (-)
n_{co2}^{out}	Mole fraction of CO_2 at the gas outlet (-)
P	Pressure (kPa)
S_G	Area of shell side (m^2)
S_L	Area of tube side(m^2)
T	Temperature (K)
v_G	Superficial gas velocity ($m.s^{-1}$)
V_G	Volume of shell side (m^3)
v_L	Superficial liquid velocity ($m.s^{-1}$)
V_L	Volume of tube side (m^3)
μ_L	Dynamic viscosity of liquid(mPa.s)
ρ_L	Density of liquid ($g.cm^{-3}$)
δ	Thickness of membrane (m)
ε_m	Porosity of membrane (-)
τ_m	Tortuosity of membrane (-)
μ_g	Viscosity of gas mixture (Pa.s)

2. Introduction

Greenhouse gas emissions (GHG) are believed to be the major contributions to the anthropogenic climate change. As the CO_2 content represents about 80% of the total greenhouse gases, CO_2 capture and storage (CCS) has been widely accepted as the most effective solution to ameliorating the rising climate temperature (Yu et al., 2008). Highly energy efficient and economically feasible technologies for CO_2 capture are desired to reduce CO_2 capture cost. Compared to post-combustion and oxy-fuel, pre-combustion process has great potential for a low energy penalty due to the high CO_2 partial pressure and hence the great separation driving force (Pardemann and Meyer, 2015). However, the severe operating conditions, such as the elevated feed gas pressure and temperature, make pre-combustion CO_2 capture process difficult. In the past few years many different capturing techniques have been studied for pre-combustion CO_2 capture, such as absorption by physical and chemical solvents, adsorption, and membrane separations (Dai et al., 2016b; Martín et al., 2011; Padurean et al., 2012; Rafiq et al., 2016; Scholes et al., 2010b).

Membrane contactor is a hybrid technology of membrane separation and solvent absorption, which offers many benefits such as high interfacial area, non-dispersive contact between the phases and avoiding flooding and foaming inside the contactor (Zhao et al., 2016). So far, a large number of different absorbents have been reported in membrane contactors for CO_2

3

capture, including amines, amino acids salts, alkaline solutions, ammonia solutions and ionic liquids (ILs) (Ansaloni et al., 2016; Mansourizadeh and Ismail, 2009; Saeed and Deng, 2016). Amine-based aqueous solvents have been mostly reported in membrane contactors for post combustions (Zhao et al., 2016). However, membrane contactors for pre-combustion CO_2 capture have been rarely reported (Chau et al., 2016; Dai et al., 2016a; Dai and Deng, 2016b; Jie et al., 2014). The use of amine-based solvents for pre-combustion operating conditions is threatened by their high volatility, large degradation rate and high corrosion rate at the elevated operating temperature. On the other hand, ILs have also been studied as promising CO_2 capture absorbents due to their unique properties such as negligible volatility, high CO_2 solubility, superior thermal stability, and tailorable structures (Zhang et al., 2012). Compared with the commercial amine-based aqueous solvents, ILs offer not only better thermal stability that ensures the high temperature application, but also negligible volatility, which leads to lower solvent loss and lower regeneration energy consumption (Zhang et al., 2017). Despite these facts, limited literatures can be found for CO_2 capture using ILs based membrane contactors (Dai et al., 2016a; Gomez-Coma et al., 2016; Gómez-Coma et al., 2014), and even less references can be found for mathematical modeling of this process (Chau et al., 2014a; Dai et al., 2016c; Gómez-Coma et al., 2016).

The mathematical models for post-CO_2 capture in membrane contactor has been addressed intensively using aqueous amine solutions to predict the separation performance and applicability range. Four types of modeling strategies are discussed and critically accessed by Chabanon et al. (Chabanon et al., 2013). Mathematical models based on constant overall mass transfer coefficient, one dimensional (1D), 1-2 dimensional and two dimensional (2D) were developed to foresee the membrane contactor performance. Constant overall mass transfer coefficient model takes into account the different mass transfer mechanisms in one parameter, i.e., the overall mass transfer coefficient (K_{ov}), which makes the model very simple and performance is accessed quickly. The limitation of constant K_{ov} model lies when loaded inlet solution would be used and CO_2 concentration profile doesn't decrease exponentially due to change in liquid side mass transfer. In another study, 1D and 2D models are equated by Albarracin et al for isothermal and adiabatic conditions, respectively (Albarracin Zaidiza et al., 2015; Albarracin Zaidiza et al., 2014). According to their findings, 1D and 2D model approaches provide quite similar results and relative difference of 2.88 % was found between both methodologies.

In our prior work, a membrane contactor process with closed cycle and continues flow using ILs as absorbent has been developed for pre-combustion CO_2 capture (Dai and Deng, 2016b). Experimental study on the CO_2 capture performances of the system has been investigated using a tubular SPG glass membrane and [Bmim][TCM] as absorbent at elevated temperature (RT~80 °C) and pressure (1~20 bar) conditions. However, the experimental study has limitations in investigating a broader range of the operating conditions or various membrane configurations (e.g., membrane length). Mathematical modeling can be a powerful tool to understand the mass transfer in the system, as well as to reduce the cost of optimization of the membrane contactor geometry and different operational parameters.

The present work aims to develop a mathematical model to simulate the CO_2 capture using ILs based membrane contactor at pre-combustion conditions (elevated temperature and pressure). The model developed in the current study will be integrated into Aspen HYSYS® for process simulation to further assess the economic feasibility of this process. The 1D model is built based on resistance in series model and mass balance in Matlab. A new mass transfer resistance term is added into the resistance in series model considering the very viscous liquid flow and the transport resistance in the liquid phase. The model was firstly validated with experimental data with this resistance term. Later on, the separation performances of the membrane contactor under different operational conditions were predicted, including gas/liquid flow rate, operational pressure/temperature, membrane wetting ratio and CO_2 concentration in the feed gas. The effect of membrane length on CO_2 capture efficiency was also investigated.

3. System Characteristics

Mass transfer of CO_2 in a membrane contactor is illustrated in Figure 1. The CO_2 gas molecules diffuse from the bulk gas phase to membrane-gas interface, pass through the pores of membrane and finally being absorbed into absorbent in the liquid phase.

The membrane contactor in this work consists of one centered tubular glass membrane in a tubular module with specifications given in Table 1. The porous SPG glass membrane is chosen on the basis of its high thermal stability and hydrophobic nature. The gas flows from the shell side and liquid passes through lumen side following parabolic velocity profile in counter current direction.

5

4. Model development

A 1D- mathematical model is developed to evaluate the mass transfer in gas-liquid tubular membrane contactor. As the solubility of H_2 in ionic liquids is remarkably lower compared to CO_2 reported, the Henry's constant of H_2 was not considered for modelling of membrane contactor. The experimental data for physical absorbent 1-Butyl-3-methylimidazolium Tricyanomethanide ([Bmim][TCM]) is mainly taken from ref (Gurkan et al., 2013). Some assumptions are made to simplify the model as follows:

- Steady state
- Isothermal process
- Concentration gradient considered in axial direction only
- Membrane acts as a non-selective barrier
- Uniform membrane pore distribution
- Laminar liquid and gas flows in tube and shell sides
- Henry's law used to represent the gas-liquid equilibrium
- Convective contributions neglected
- Fick's diffusion applied for membrane mass transfer

The simplified block diagram of the model development is represented in the Figure 2.

The physicochemical properties of [Bmim][TCM] and gases are presented in Tables 2 (a) and (b).

A mathematical 1D-model has been developed by applying the mass balance over the tubular membrane contactor, which is portioned mainly into the gas, membrane and liquid sides. The steady state mass balance over the membrane contactor gives the following equations for gas and liquid sides:

Gas phase molar balance

$$0 = (v_G S_G\ C_{co2}^G)_z - (v_G S_G C_{co2}^G\ )_{z+dz} - N_{co2}\ dA \tag{1a}$$

$$0 = (F_G S_G)_z - (F_G S_G)_{z+dz} - N_{co2} dA \tag{1b}$$

6

$$\frac{dF_g}{dz} = -N_{co2}\left(\frac{A_m}{V_G}\right) \tag{1c}$$

Liquid phase molar balance

$$0 = (v_L S_L C_{co2}^L)_{z+dz} - (v_L S_L C_{co2}^L)_z + N_{co2}\, dA \tag{2a}$$

$$0 = (F_L S_L)_{z+dz} - (F_L S_L)_z + N_{co2} dA \tag{2b}$$

$$\frac{dF_L}{dz} = -N_{co2}\frac{A_m}{V_L} \tag{2c}$$

Where F_G and F_L are gas and liquid molar flow rates (mol/m^2.s), N_{CO2} is the mass transfer flux of CO_2 from the gas to the liquid phase through membrane, A_m is the membrane area, V_G and V_L are the volumes of shell and tube side of the membrane contactor, respectively. The CO_2 absorption flux (N_{CO2}) can be derived from the local driving forces of gas, membrane and liquid phases from equations 3, 4 and 5:

$$N_{co2,g} = k_g\left(C_{co2}^g - C_{co2}^{gm}\right) \tag{3}$$

$$N_{co2,m} = k_m\left(C_{co2}^{gm} - C_{co2}^{i,g}\right) \tag{4}$$

$$N_{co2,l} = k_l\left(C_{co2}^{i,l} - C_{co2}^l\right) \tag{5}$$

Where C_{CO2}^i stands for concentration of CO_2 at equilibrium with the liquid phase, C_{co2}^L is the concentration of CO_2 in the bulk liquid phase. The term C_{CO2}^i can be described by the dimensionless Henry's law constant as:

$$m = \frac{C_{co2}^{i,g}}{C_{co2}^{i,l}} \tag{6}$$

After introducing the dimensionless Henry's law constant, the CO_2 absorption flux in terms of overall driving force can be expressed as:

$$N_{co2} = K_{ov}\left(\frac{C_{CO2}^g}{m} - C_{co2}^l\right) \tag{7}$$

The overall mass transfer coefficient can be modeled by resistance in series model and expressed as:

$$K'_{ov} = \left(\frac{1}{mk_g} + \frac{1}{Hm} + \frac{1}{k_l}\right)^{-1} \tag{8}$$

7

k_g, k_l and k_m are defined as individual mass transfer coefficients for gas, liquid and membrane phases, respectively. These mass transfer coefficients can be estimated depend on the Reynold' number range and geometry of membrane contactor.

For the plug flow assumption, the concentration in the liquid phase follows parabolic profile and no concentration gradient is considered. However, in actual factor, there is concentration gradient due to transport resistance as presented in Figure 3 by dash line. To account for the transport resistance in the liquid phase, the concentration gradient is fitted to a second order polynomial (equation 9) in radius 'r' and inserting the boundary conditions (detailed derivation can be seen in the supporting information).

$$C = a + br + cr^2 \tag{9}$$

Boundary conditions:

At r=0, $\dfrac{dC}{dr} = 0$

At r=R, $-D\dfrac{dC}{dr} = K_{ov}^{'}(C_R - C_{cw})$

And the average concentration profile can be expressed as:

$$< C >= \frac{\int_0^R 2\pi r\, C(r)dr}{\int_0^R 2\pi r\, dr} \tag{10}$$

After solving the equation 9 and 10, the overall mass transfer coefficient follows the new form including transport resistance in liquid as:

$$K_{ov} = \frac{1}{\frac{d_i}{8D_{l,co2}} + \frac{1}{K_{ov}^{'}}} \tag{11}$$

In which d_i represents the membrane inner diameter and $D_{l,CO2}$ denotes the diffusivity of CO_2 in liquid phase.

8

3.1 Liquid side mass transfer coefficient

The liquid flow rate used in the experimental setup is in quite low range (20 mL/min), resulted in a small Reynold's number. In this case, the liquid side mass transfer coefficient (k_l) can be well estimated by the correlation given by Yang and Cussler (Yang and Cussler, 1986):

$$k_l = 1.62 \, Re_l^{0.33} Sc_l^{0.33} \left(\frac{d_i}{L}\right)^{0.33} \left(\frac{D_{l,co2}}{d_i}\right) \tag{12}$$

L and di define the length and inner diameter of membrane contactor respectively while $D_{CO2,l}$ stands for CO_2 diffusivity in liquid phase.

3.2 Gas side mass transfer coefficient

The gas flows in the shell side and the gas side mass transfer coefficients is proposed by (Yang and Cussler, 1986):

$$k_g = 1.25 Re_g^{0.93} Sc_g^{0.33} \left(\frac{d_h}{L}\right)^{0.93} \left(\frac{D_{co2,g}}{d_h}\right) \tag{13}$$

Where $D_{CO2,g}$ denotes the diffusivity of CO_2 in gas phase and d_h the hydraulic diameter of shell.

3.3 Membrane mass transfer coefficient

Membrane side mass transfer coefficient based on non-wetted and wetted modes can be presented by equation 14:

$$k_m = \frac{1}{\frac{1}{k_{m,g}}(1-\varphi)+\frac{1}{k_{m,l}}(\varphi)} \tag{14}$$

The term φ in equation 14 represents the wetting ratio of membrane pores. $k_{m,g}$ is the membrane mass transfer coefficient for the non-wetted mode and $k_{m,l}$ represents for the wetted mode and are given by equations 15 and 16.

$$k_{m,g} = \frac{D_{co2,m}\epsilon_m}{\delta_m \tau_m} \tag{15}$$

$$k_{m,l} = \frac{D_{co2,l}\epsilon_m}{\delta_m \tau_m} \tag{16}$$

ϵ_m, δ_m, τ_m represents the membrane porosity, thickness and tortuosity. $D_{CO2,m}$ denotes the CO_2 diffusivity in the membrane phase.

The diffusion in membrane phase can take place by two mechanisms, namely molecular diffusion and Knudsen diffusion. Molecular diffusion takes place when the pore size is larger than 10^{-5} m and Knudsen diffusion occurs for membrane pore size less than 10^{-7}m. In our case, both molecular diffusion and Knudsen diffusion happens in the membrane phase. Thus, the CO_2 diffusion coefficient in the membrane phase can be expressed as:

$$D_{co2,m} = \frac{1}{\left(\frac{1}{D_{co2,mol}}+\frac{1}{D_{co2,kn}}\right)} \tag{17}$$

The molecular diffusion coefficient ($D_{CO2,mol}$) can be calculated as given in table 2b while Knudsen diffusion coefficient ($D_{CO2,kn}$)can be estimated by (Boributh et al., 2011):

$$D_{co2,kn} = \frac{d_p}{3}\sqrt{\frac{8\times10^6 RT}{\pi M_{co2}}} \tag{18}$$

3.4 Pressure drop

Pressure drop is a critical parameter in determining mass transfer characteristics of a membrane contactor. If the pressure drop along the membrane module overtake the critical entry pressure of the membrane pores, it may cause bubbling or membrane wetting, both case will dramatically decrease the membrane separation efficiency. Pressure drop in the glass membrane contactor is predicted by a well-known correlation of Hagen- Poiseuille's for laminar shell and tube side:

$$\Delta P_g = -\frac{32\,\mu_g\,v_g\,L}{d_h^2} \tag{19}$$

$$\Delta P_l = -\frac{32\,\mu_l\,v_l\,L}{d_i^2} \tag{20}$$

The v_g and v_l represent gas and liquid velocities, μ_g and μ_l represent viscosity of gas and liquid respectively.

5. Numerical solution

The developed equations for gas, liquid and membrane phases are ordinary differential equations with defined boundary values. These equations are solved by the collocation method in MATLAB program. The collocation method is subclass of method of weighted residuals which solves the boundary value problem. It yields discrete approximations to differential

10

operators by converting them into polynomials. The set of non-linear polynomial equations of several variables are then solved by f-solve routine in MATLAB.

6.   Results and discussion

5.1 Model validation

The experimental study using [Bmim][TCM] as absorbent was performed in a tubular glass membrane contactor in our previous work (Dai and Deng, 2016a). The developed model was validated by comparing the CO_2-outlet concentration from the experimental data at different temperatures and pressures. The results are shown in Figure 4. The accuracy limit of the experimental and modeling data was estimated by the absolute average overall deviation (AARD), which is computed as:

$$AARD = \frac{1}{N}\sum_{i=1}^{N} 100 \; \frac{|C_{co2,mod}^{out} - C_{co2,exp}^{out}|}{C_{co2,exp}^{out}} \qquad (21)$$

It can be clearly observe from Figure 4 that the model (solid line) shows a good agreement with the experimental results over the whole operating pressure range (1~20 bar), and even smaller deviations can be found at lower operating pressure conditions (up to 5bar), where the AARD value is always lower than 3 %. The AARD value is bigger (4 - 8%) at higher pressures (10-20bar), especially at lower temperatures. The AARD value in this work is comparable with other reports. For example, Chau et al. studied the separation of shifted syngas CO_2 separation from H_2 using a physical absorbent in membrane contactor (Chau et al., 2014b). They compared the experimental and modelling results, and AARD values of 4 - 9 % were obtained in the temperature range of 25-100 °C at 10 bar.

This deviation can be attributed to the correlations used to estimate the physical properties of gas and liquid phases, which is rarely extended to our operating pressure (up to 20 bar) and temperature (up to 80 °C) conditions. In addition, Helium is used as surrogate of H_2 in the experimental work due to safety issues, which may slightly vary both in gas solubility and diffusivity.

The deviation from experimental results becomes more significant as pressure increases to 20 bar, where the maximum deviation value of 8 % was noted for the case of pressure at 20 bar

11

and temperature at 22 ºC. At low temperatures, the ionic liquid was quite viscous and it was challenging to run the experiments at low temperatures. This could have resulted in a bigger deviation of experimental values from model prediction. As the liquid side mass transfer resistance is dominating, the high viscosity of liquid and thus the low diffusivity of CO_2 in the liquid are the key factors of this deviation. As [Bmim][TCM] possesses a higher viscosity (30 mPa.s) compared to conventional aqueous amine solvents, the diffusivity of CO_2 in the liquid phase in this system is lower.

Another prime reason for the deviation could be the pore wetting of the membrane (dash line in Figure 4). As the membrane contactor is operated at elevated pressure conditions, the control of the pressure over the membrane between gas and liquid phases is difficult. A slight drafting of the pressure difference away from the optimal pressure range could give rise to pore wetting. Pore wetting has been observed in experiment as reported in our previous study (Dai and Deng, 2016b). In addition, the contact angle of the membrane surface decreased after several experimental runs, which makes the pore wetting more serious. Thus, the pore wetting was considered in the model and it improved the accuracy of the prediction of CO_2-outlet values. In this case, model predicted the experimental data with the AARD of only about 1.4%. This confirmed the pore wetting in the membrane.

5.2 Axial concentration profiles of CO_2 in gas phase

The model predicts the concentration profiles for CO_2 in gas phase along the axial length of membrane contactor, as illustrated in Figure 5. The dimensionless concentration of CO_2 in gas phase decreases along the length of the membrane contactor. The gas enters the contactor at position z=0 and leaves at z=L. The CO_2 concentration at z=0 shows the maximum value (1) and reduces to 0.78 at the gas outlet (z=L). The percentage decrease in the gas phase concentration is recorded to be 22%. It means that about 22% of CO_2 from the gas phase has passed into the liquid phase through a tubular membrane of 0.26m in length.

First, there is steady decrease in the concentration and then sharply reduces after the half-length of the membrane contactor. This total amount of CO_2 transport through the membrane phase can be enhanced by increasing the length of membrane contactor. The length of membrane contactor can be optimized based on the CO_2 capture efficiency.

The effect of membrane contactor length on CO_2 capture efficiency is also studied, as presented in Figure 6. The CO_2 capture efficiency is calculated as described in equation 22, and other

operational parameters such as gas and liquid flow rates, temperature and pressure are kept constant.

$$\eta = \frac{(n_{co2}^{in} - n_{co2}^{out})}{n_{co2}^{in}} \times 100 \qquad (22)$$

The increase of membrane contactor length up to 1.0 m results in an increase in CO_2 capture efficiency, and then the influence of the length becomes less and less significant, and finally the plot is almost flattened. It indicates that maximum CO_2 absorption efficiency (18%) can be achieved with these operational conditions. The liquid and gas flow rates also affect in determining the length of the membrane contactor. The optimal length of membrane contactor can be estimated for specific operating conditions.

5.3 Axial profile of CO_2 absorption flux

The mass transfer performance of many gas-liquid contacting device has usually been reported in the term of CO_2 absorption flux. In this work, the CO_2 absorption flux in [Bmim][TCM] along the length of the glass tubular membrane contactor is calculated from equation 7, as presented in Figure 7.

The CO_2 absorption flux at the gas inlet (z=0) is $5.28E^{-5}$ mol $m^{-2}s^{-1}$ and it increases to $9.62E^{-5}$ mol $m^{-2}s^{-1}$ as the gas passes through the membrane contactor. The absorption flux is quite comparable with aqueous amine and alkali (NaOH) solutions based membrane contactors (Marzouk et al., 2012; Zhang et al., 2006). For instance, Zhang observed the absorption flux in the range of 10^{-4} mol $m^{-2}s^{-1}$ for 2M DEA aqueous solution at atmospheric pressure. Marzouk et al.(Marzouk et al., 2012) studied the removal of CO_2 and H_2S using NaOH solutions at high pressure conditions. The absorption flux values are in the range of 10^{-4}-10^{-3} mol/m^2.s, which are 10 times higher than the flux achieved in this case. The difference in the flux values could have stemmed from chemical reaction between absorbent and CO_2 in these cases, while physical absorbent is used in our study. Another reason could be the much higher viscosity of the IL absorbent than the aqueous solutions.

5.4 Assessment of mass transfer resistances

The resistance caused by the boundary wall layer is considered in the present study. Individual mass transfer resistances for each phase are represented in Table 4 both for wetted and non-wetted conditions.

These mass transfer resistances are tabulated for 20 bar pressure and 80 °C temperature. The liquid phase mass transfer resistance is the controlling step as it dominates the overall mass transfer resistances by contributing up to 67 % to the overall resistance. The liquid side mass transfer coefficient is proportional to the CO_2 diffusivity in a liquid phase. The diffusivity correlation used for the estimation incorporates the liquid viscosity as inverse function. At room temperature, the viscosity of [Bmim][TCM] is quite high (31 mPa.s) compared to many other physical absorbents for CO_2 capture. For example, viscosity if max 5.8 mPa.s was reported for selexol solvent (Chabanon et al., 2014). The viscosity of [Bmim][TCM] reduces to 5 mPa.s at 80 °C. Another parameter that influences the liquid side resistance is the liquid velocity. However, the liquid flowrate in experiments was fixed at 20 mL min^{-1} in this work as discussed earlier.

The other prominent resistance term that accounts 31 % of the total resistance is due to transport resistance in liquid phase as described in section 3. This resistance term takes into account the diffusivity of CO_2 in liquid, which is quite low due to the high viscosity of [Bmim][TCM]. Surprisingly, the membrane mass transfer resistance is the least (0.022 %) among all resistances for non-wetted mode of operation, but it takes up 34 % in the total resistance for the wetted membrane case. Consequently, the liquid and membrane resistances dominates the mass transfer in case of wetted membrane mode.

The contribution of the different mass transfer steps suggest that to reduce the liquid phase resistance is the most effective approach, and membrane pores should be kept non-wetted. The liquid phase resistance may be reduced by increasing the liquid velocity; The effect of liquid flow rate on overall mass transfer flux will be presented in section 5.6. Liquid side mass transfer coefficient is also inversely dependent on its viscosity. To reduce the liquid phase viscosity, blend IL absorbent with low viscous co-solvent, such as low molecular weight PEG (Li et al., 2016; Usman et al., 2016), can be used.

5.5 Effect of pressure and temperature on CO_2-capture efficiency

It has been widely reported that the operational pressure and temperature have significant influence on the mass transfer for both physical and chemical absorptions. However, so far most of the reported literature covers the post-combustion CO_2 capture that operates at atmospheric pressure. In this work, the separation is at pre-combustion conditions, and CO_2 partial pressure is much higher. The increase in pressure could enhance the driving force for mass transfer and result in higher mass transfer flux. In order to analyze the performance of

membrane contactor, the CO_2-capture efficiency (η) is calculated for different pressure and temperature values by equation 22 and results are presented in Figure 8.

The CO_2-capture efficiency shows a linear increasing trend with respect to pressure. The pressure increase enhances the CO_2 mass transfer driving force and thus the absorption flux, resulting in a larger CO_2-capture efficiency. It showed an increment of about 11% in CO_2-capture efficiency by increasing the pressure to 20 bar from atmospheric pressure. On the other hand, the CO_2-capture efficiency is slightly reduced from 11 % to 9 % by increment in temperature. There is no appreciable change in the CO_2-capture efficiency at atmospheric pressure to 10 bar for all temperatures and the same trend was observed during the experimental run for CO_2 flux values as reported in (Dai and Deng, 2016a). It can be concluded that temperature has negligible effect on the CO_2-capture efficiency compared to the pressure. The lower viscosity of the liquid at high temperatures resulted in low liquid side mass transfer resistance but at the same time the solubility of CO_2 in ionic liquid also decreased by increasing the temperature. From these observations, it can be proposed that the CO_2 capture efficiency showed maximum at 20bar pressure and 293.15K. However, the viscosity of ionic liquid will get lower at higher temperature and become comparable to other physical absorbents such as polypropylene carbonate, methanol and DMEPEG (Chabanon et al., 2014). Thus, the influence of temperature should be considered in the design of this membrane absorption-desorption process.

5.6 Effect of gas and liquid flow rates on contactor performance

Operational parameters such as liquid and gas flow rates determine the performance of gas-liquid contacting device and these affect the CO_2 capture efficiency and overall mass transfer. Sensitivity of these parameters is investigated in this section. Figures 9 (a, b) illustrate the effect of gas and liquid flow rates on CO_2 absorption flux. The liquid flow rate was fixed to 20 mL min^{-1}, and CO_2 absorption flux and thickness of boundary layer were estimated in a gas flow rate range of 20 to 350 mL min^{-1}.

Thickness of liquid boundary layer is defined as:

$$\delta_{B.L}(m) = \frac{D_{l,co2}}{k_l} \qquad (23)$$

As shown in Figure 9 (a), the CO_2 absorption flux increases from 6.52E-05 mol m^{-2} s^{-1} to 1.11E-04 mol m^{-2} s^{-1} with increasing the gas flow rate from 20 to 350 mL min^{-1}. The CO_2 absorption flux firstly boosted at up to 150 mL min^{-1} and then it improvement becomes much slower at a higher gas flow rate. Therefore, further increase in the gas flow rate didn't improve the absorption process.

The effect of liquid velocity on CO_2 flux is also investigated. The results are shown in Figure 9 (b). As can be seen, increasing liquid flow rate can reduce the liquid boundary layer thickness and increase CO_2 absorption flux. Increasing the liquid flow rate from 56 ml min^{-1} to 350 ml min^{-1} results in the improvement of the CO_2 absorption flux for about 24 %, and the reduction in the boundary layer thickness for approximately 60 %. Due to the large driving force at 20 bar, it can be reasonable to conclude that the effect of liquid flow rate on enhancing the CO_2 absorption flux is more significant than that of the gas flow rate. The optimum gas and liquid flow rates can be estimated for the maximum achievable absorption flux in the membrane contactor.

5.7 Effect of CO_2 concentration in feed gas

The CO_2 concentration in syngas may vary from 30% to 55% (Scholes et al., 2010a). Therefore, it is important to analyze how CO_2 concentration in syngas can affect the membrane contactor performance. Figure 9 represents the CO_2-capture efficiency as a function of CO_2 gas concentration (%) in the feed for wetted and non-wetted conditions. The feed with higher CO_2 concentration resulted in greater CO_2-capture efficiency values for both the cases.

The increment in concentration of CO_2 in feed gas lifts the partial pressure of CO_2 and concentration gradient increases at the interface. This produces the enhanced CO_2 absorption flux, and better CO_2-capture efficiency is obtained. There is roughly an increment of about 47% in CO_2 capture efficiency with the feed gas concentration increasing from 30% to 55% for both modes of operation. Overall, the captured CO_2 is reduced to 25% for wetted mode compared to that of the non-wetted mode at 50% feed gas concentration. The membrane resistance would add to the overall mass transfer significantly for wetted mode, and thus less CO_2 will be absorbed.

7. Conclusions

A one dimensional (1D) mathematical model was developed to analyze the mass transfer and CO_2 capture performance of an ILs based membrane contactor at elevated temperatures and pressures. The model predicted the CO_2 concentration at the gas outlet and the simulation results were validated with the experimental data, showing the accuracy of the model with the AARD value in the range of 0 - 8 %. The axial profiles for CO_2 concentration and CO_2 absorption flux were predicted along the length of membrane contactor.

The simulation results reveal the following facts:

(1) The pressure and CO_2 concentration in the feed give more significant influence on the CO_2 capture efficiency than the operating temperature;

(2) The increase in the gas/liquid flow rate could reduce the gas/liquid film boundary layer thickness and thus increase the CO_2 absorption flux;

(3) Increasing membrane length can increase the CO_2 capture efficiency, and CO_2 absorption flux increased by two-fold with increment in length of membrane contactor up to 1m.

Acknowledgments

References

Albarracin Zaidiza, D., Belaissaoui, B., Rode, S., Neveux, T., Makhloufi, C., Castel, C., Roizard, D., Favre, E., 2015. Adiabatic modelling of CO2 capture by amine solvents using membrane contactors. J Membrane Sci 493, 106-119.

Albarracin Zaidiza, D., Billaud, J., Belaissaoui, B., Rode, S., Roizard, D., Favre, E., 2014. Modeling of CO2 post-combustion capture using membrane contactors, comparison between one- and two-dimensional approaches. J Membrane Sci 455, 64-74.

Ansaloni, L., Arif, A., Ciftja, A.F., Knuutila, H.K., Deng, L., 2016. Development of Membrane Contactors Using Phase Change Solvents for CO2 Capture: Material Compatibility Study. Ind Eng Chem Res 55, 13102-13113.

Boributh, S., Assabumrungrat, S., Laosiripojana, N., Jiraratananon, R., 2011. A modeling study on the effects of membrane characteristics and operating parameters on physical absorption of CO2 by hollow fiber membrane contactor. J Membrane Sci 380, 21-33.

Chabanon, E., Belaissaoui, B., Favre, E., 2014. Gas-liquid separation processes based on physical solvents: opportunities for membranes. J Membrane Sci 459, 52-61.

Chabanon, E., Roizard, D., Favre, E., 2013. Modeling strategies of membrane contactors for post-combustion carbon capture: A critical comparative study. Chem Eng Sci 87, 393-407.

Chau, J., Jie, X., Sirkar, K.K., 2016. Polyamidoamine-facilitated poly (ethylene glycol)/ionic liquid based pressure swing membrane absorption process for CO 2 removal from shifted syngas. Chemical Engineering Journal 305, 212-220.

Chau, J., Obuskovic, G., Jie, X., Sirkar, K.K., 2014a. Pressure swing membrane absorption process for shifted syngas separation: Modeling vs. experiments for pure ionic liquid. J Membrane Sci 453, 61-70.

Chau, J., Obuskovic, G., Jie, X.M., Sirkar, K.K., 2014b. Pressure swing membrane absorption process for shifted syngas separation: Modeling vs. experiments for pure ionic liquid. J Membrane Sci 453, 61-70.

Dai, Z., Ansaloni, L., Deng, L., 2016a. Precombustion CO2 Capture in Polymeric Hollow Fiber Membrane Contactors Using Ionic Liquids: Porous Membrane versus Nonporous Composite Membrane. Ind Eng Chem Res 55, 5983-5992.

Dai, Z., Ansaloni, L., Deng, L., 2016b. Recent advances in multi-layer composite polymeric membranes for CO2 separation: A review. Green Energy & Environment 1, 102-128.

Dai, Z., Deng, L., 2016a. Membrane absorption using ionic liquid for pre-combustion CO2 capture at elevated pressure and temperature. International Journal of Greenhouse Gas Control 54, Part 1, 59-69.

Dai, Z., Deng, L., 2016b. Membrane absorption using ionic liquid for pre-combustion CO 2 capture at elevated pressure and temperature. International Journal of Greenhouse Gas Control 54, 59-69.

Dai, Z., Usman, M., Hillestad, M., Deng, L., 2016c. Modelling of a tubular membrane contactor for pre-combustion CO 2 capture using ionic liquids: Influence of the membrane configuration, absorbent properties and operation parameters. Green Energy & Environment.

Fuller, E.N., Schettle, P.D., Giddings, J.C., 1966. A New Method for Prediction of Binary Gas-Phase Diffusion Coeffecients. Ind Eng Chem 58, 19-+.

Gomez-Coma, L., Garea, A., Irabien, A., 2016. Carbon dioxide capture by [emim][Ac] ionic liquid in a polysulfone hollow fiber membrane contactor. International Journal of Greenhouse Gas Control 52, 401-409.

Gómez-Coma, L., Garea, A., Irabien, A., 2014. Non-dispersive absorption of CO 2 in [emim][EtSO 4] and [emim][Ac]: temperature influence. Separation and Purification Technology 132, 120-125.

Gómez-Coma, L., Garea, A., Irabien, A., 2016. PVDF MEMBRANE CONTACTOR FOR CO2 CAPTURE USING THE IONIC LIQUID [emim][Ac]: MASS TRANSFER ANALYSIS. Chemical Engineering & Technology, n/a-n/a.

Gurkan, B.E., Gohndrone, T.R., McCready, M.J., Brennecke, J.F., 2013. Reaction kinetics of CO2 absorption in to phosphonium based anion-functionalized ionic liquids. Phys Chem Chem Phys 15, 7796-7811.

Jie, X., Chau, J., Obuskovic, G., Sirkar, K.K., 2014. Enhanced Pressure Swing Membrane Absorption Process for CO2 Removal from Shifted Syngas with Dendrimer–Ionic Liquid Mixtures as Absorbent. Ind Eng Chem Res 53, 3305-3320.

Li, J., Dai, Z., Usman, M., Qi, Z., Deng, L., 2016. CO2/H2 separation by amino-acid ionic liquids with polyethylene glycol as co-solvent. International Journal of Greenhouse Gas Control 45, 207-215.

Lucas, K., 1980. Review of present status of transport properties prediction, Phase equilibria and fluid properties in the chemical industry.

Mansourizadeh, A., Ismail, A.F., 2009. Hollow fiber gas–liquid membrane contactors for acid gas capture: a review. Journal of hazardous materials 171, 38-53.

Martín, C.F., Stöckel, E., Clowes, R., Adams, D.J., Cooper, A.I., Pis, J.J., Rubiera, F., Pevida, C., 2011. Hypercrosslinked organic polymer networks as potential adsorbents for pre-combustion CO 2 capture. Journal of Materials Chemistry 21, 5475-5483.

Marzouk, S.A.M., Al-Marzouqi, M.H., Teramoto, M., Abdullatif, N., Ismail, Z.M., 2012. Simultaneous removal of CO2 and H2S from pressurized CO2-H2S-CH4 gas mixture using hollow fiber membrane contactors. Separation and Purification Technology 86, 88-97.

Morgan, D., Ferguson, L., Scovazzo, P., 2005. Diffusivities of gases in room-temperature ionic liquids: Data and correlations obtained using a lag-time technique. Industrial & Engineering Chemistry Research 44, 4815-4823.

Padurean, A., Cormos, C.-C., Agachi, P.-S., 2012. Pre-combustion carbon dioxide capture by gas–liquid absorption for integrated gasification combined cycle power plants. International Journal of Greenhouse Gas Control 7, 1-11.

Pardemann, R., Meyer, B., 2015. Pre-Combustion Carbon Capture, Handbook of Clean Energy Systems. John Wiley & Sons, Ltd.

Rafiq, S., Deng, L., Hägg, M.-B., 2016. Role of Facilitated Transport Membranes and Composite Membranes for Efficient CO2 Capture – A Review. ChemBioEng Reviews 3, 68-85.

Saeed, M., Deng, L., 2016. Post-combustion CO2 membrane absorption promoted by mimic enzyme. J Membrane Sci 499, 36-46.

Scholes, C.A., Smith, K.H., Kentish, S.E., Stevens, G.W., 2010a. CO2 capture from pre-combustion processes—Strategies for membrane gas separation. International Journal of Greenhouse Gas Control 4, 739-755.

Scholes, C.A., Smith, K.H., Kentish, S.E., Stevens, G.W., 2010b. CO 2 capture from pre-combustion processes—strategies for membrane gas separation. International Journal of Greenhouse Gas Control 4, 739-755.

Usman, M., Huang, H., Li, J., Hillestad, M., Deng, L., 2016. Optimization and Characterization of an Amino Acid Ionic Liquid and Polyethylene Glycol Blend Solvent for Precombustion CO2 Capture: Experiments and Model Fitting. Industrial & Engineering Chemistry Research 55, 12080-12090.

Yang, M.-C., Cussler, E.L., 1986. Designing hollow-fiber contactors. Aiche Journal 32, 1910-1916.

Yu, K.M.K., Curcic, I., Gabriel, J., Tsang, S.C.E., 2008. Recent Advances in CO2 Capture and Utilization. Chemsuschem 1, 893-899.

Zhang, H.Y., Wang, R., Liang, D.T., Tay, J.H., 2006. Modeling and experimental study of CO2 absorption in a hollow fiber membrane contactor. J Membrane Sci 279, 301-310.

Zhang, X., Bai, L., Zeng, S., Gao, H., Zhang, S., Fan, M., 2017. Ionic Liquids: Advanced Solvents for CO2 Capture, in: Budzianowski, W.M. (Ed.), Energy Efficient Solvents for CO2 Capture by Gas-Liquid Absorption: Compounds, Blends and Advanced Solvent Systems. Springer International Publishing, Cham, pp. 153-176.

Zhang, X., Zhang, X., Dong, H., Zhao, Z., Zhang, S., Huang, Y., 2012. Carbon capture with ionic liquids: overview and progress. Energy & Environmental Science 5, 6668-6681.

Zhao, S., Feron, P.H., Deng, L., Favre, E., Chabanon, E., Yan, S., Hou, J., Chen, V., Qi, H., 2016. Status and progress of membrane contactors in post-combustion carbon capture: A state-of-the-art review of new developments. J Membrane Sci 511, 180-206.

Zubeir, L.F., Romanos, G.E., Weggemans, W.M.A., Iliev, B., Schubert, T.J.S., Kroon, M.C., 2015. Solubility and Diffusivity of CO2 in the Ionic Liquid 1-Butyl-3-methylimidazolium Tricyanomethanide within a Large Pressure Range (0.01 MPa to 10 MPa). J Chem Eng Data 60, 1544-1562.
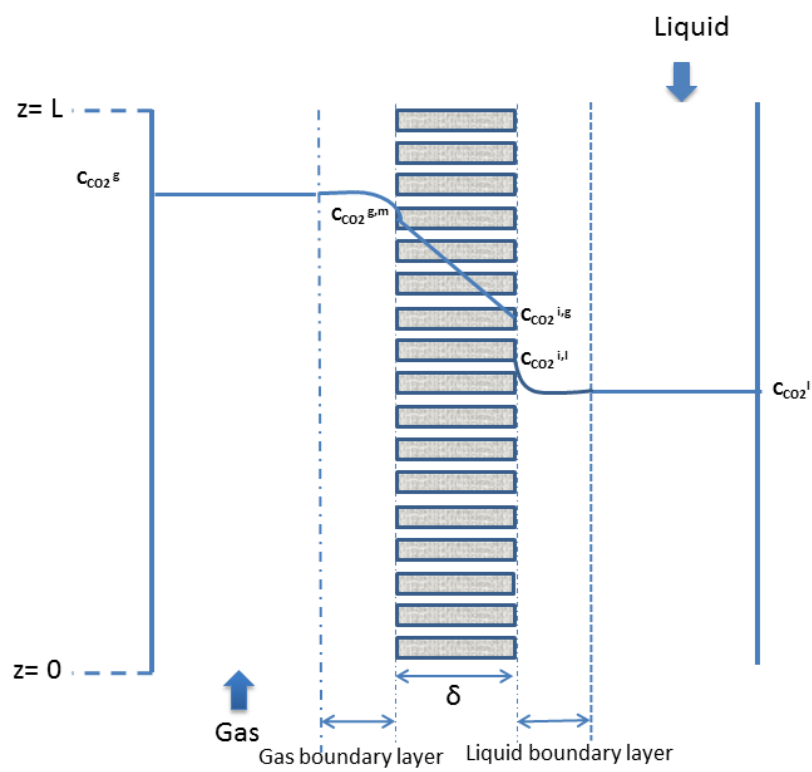
Figure 1. Schematic representation of a gas-liquid membrane contactor
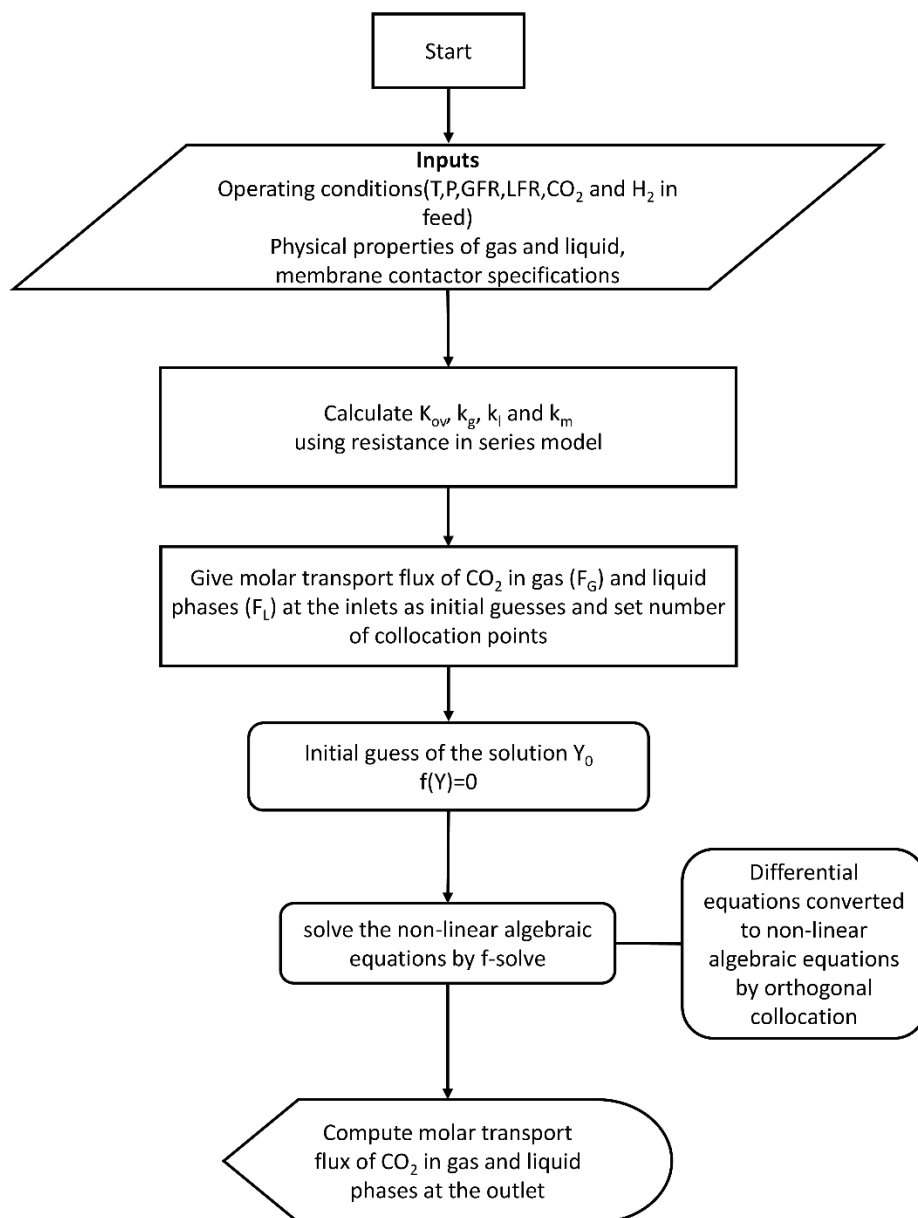
Figure 2. Simplified block diagram of the mathematical model
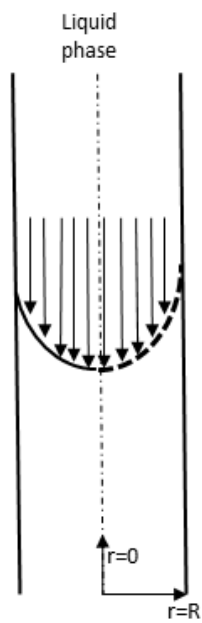
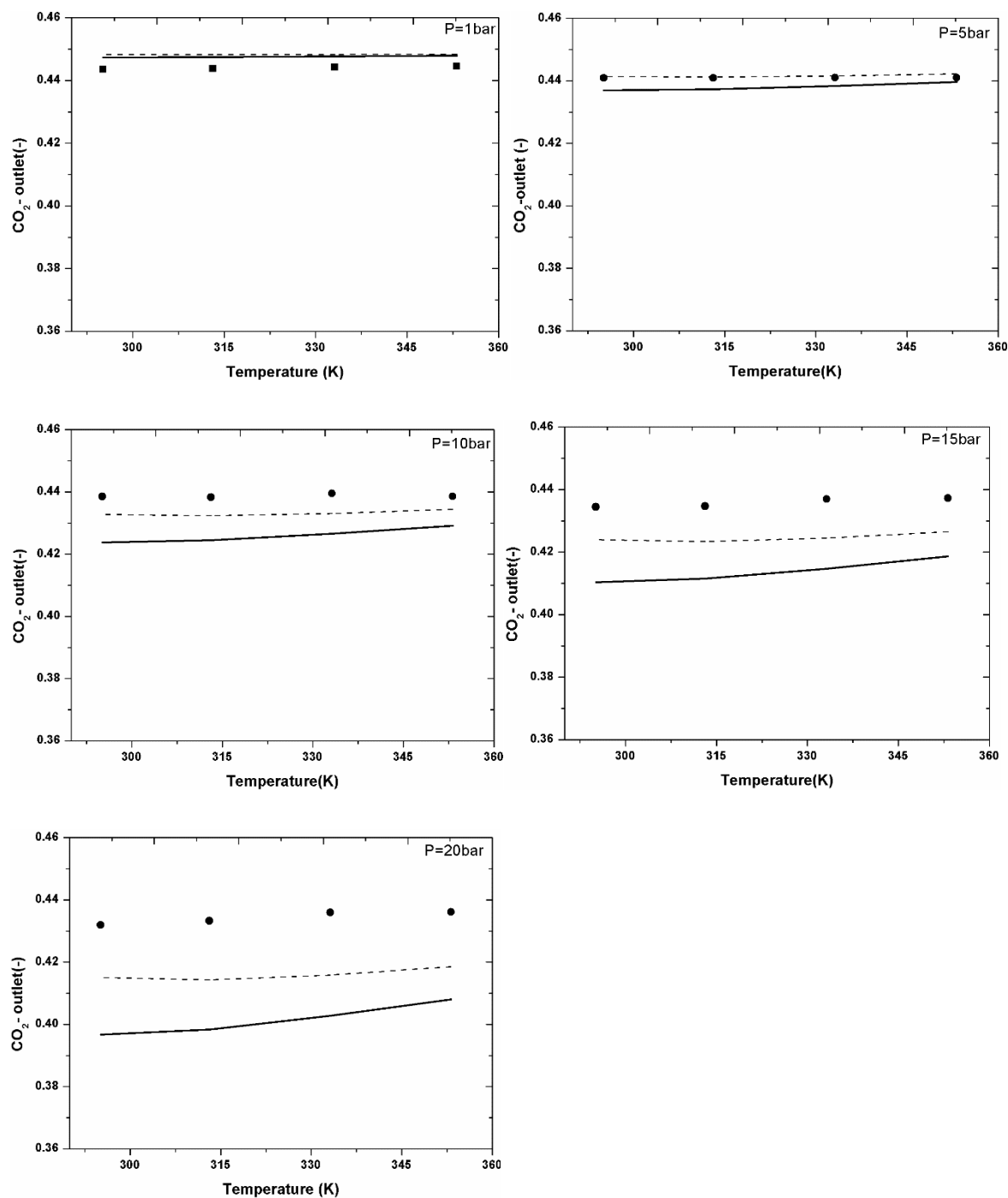Figure 3. The concentration profile in the liquid phase

Figure 4. Model validation for CO_2-outlet concentration as function of temperature for completely wetted and non-wetted membrane modes; experiments (round symbol), model-wetted mode (dash line), model-non-wetted mode (solid line). Gas flow rate=56 mL min-1, liquid flow rate=20 mL min-1
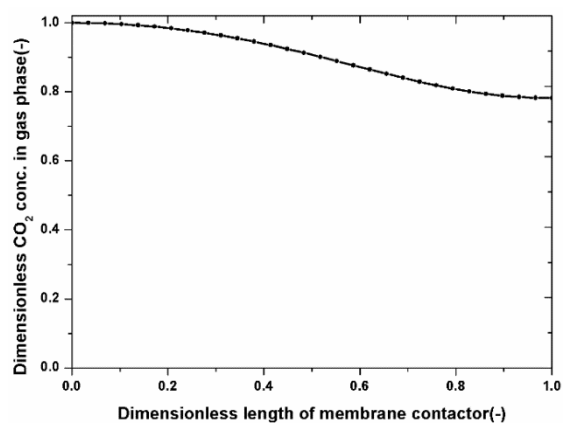
Figure 5. Concentration of CO_2 in the gas phase along the axial coordinates. Temperature=80 $^{\circ}$C, pressure=20 bar, gas flow rate=56 mL min-1, liquid flow rate=20 mL min^{-1}, effective membrane length=260 mm.
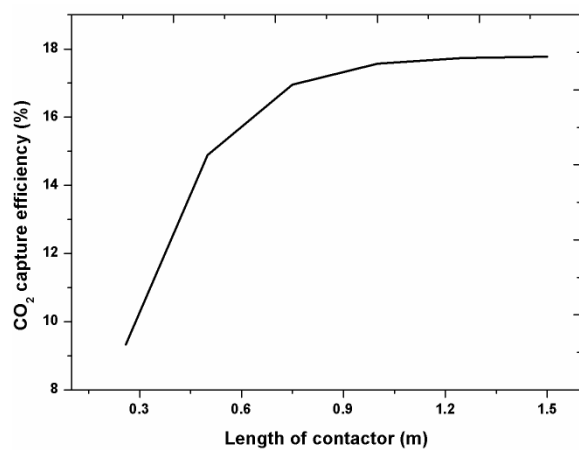
Figure 6. Effect of length of membrane contactor on CO_2 capture efficiency; pressure=20 bar, temperature=80 ºC, gas flow rate=56 mL/min, liquid flow rate=20 mL/min
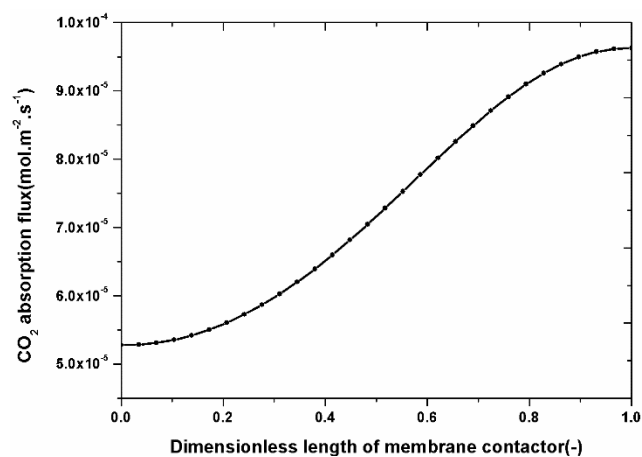
Figure 7. Absorption flux of CO_2 in liquid absorbent along the length of membrane contactor. Temperature=80 ºC, pressure=20 bar, gas flow rate=56 mL min^{-1}, liquid flow rate=20 mL min^{-1}
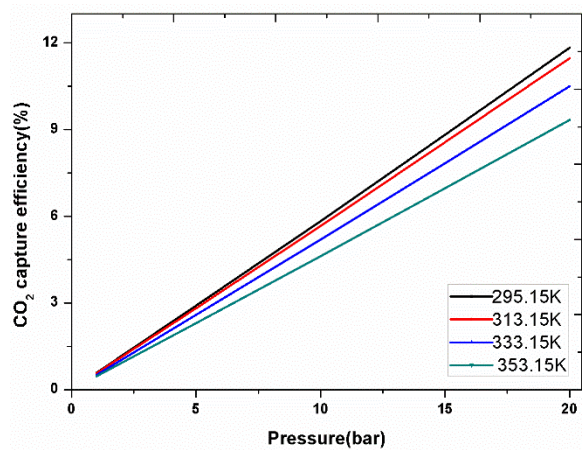
Figure 8. Influence of system pressure on CO_2-capture efficiency in membrane contactor; gas flow rate=56 mL min-1, liquid flow rate=20 mL min^{-1}
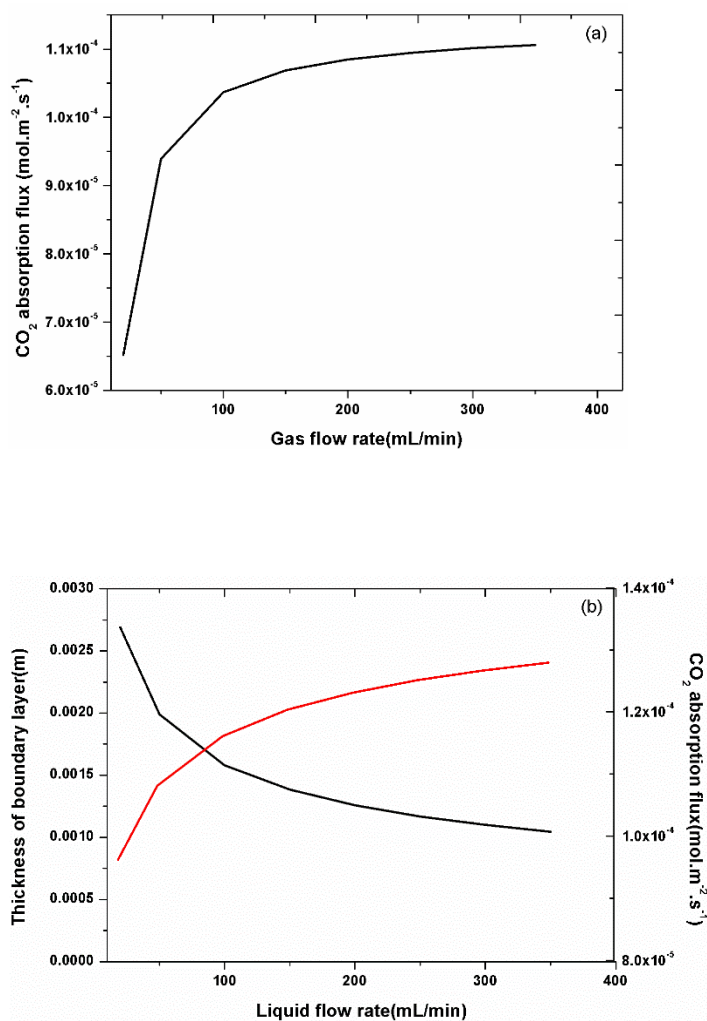
Figure 9. The effect of gas flow rate (a) and liquid flow rate (b) on CO_2 mass transfer flux; pressure=20 bar, temperature=80 ^oC, gas flow rate= 56 mL min^{-1}
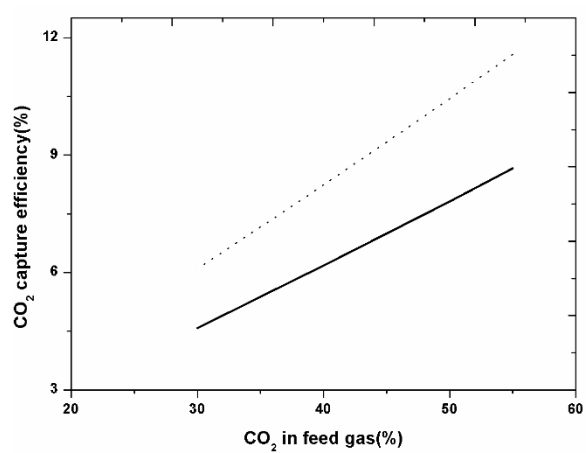
Figure 9. The effect of CO_2 concentration in feed syngas on CO_2- efficiency for non-wetted (solid line) and wetted modes (dash line); pressure=20 bar, temperature=80 $^{\circ}$C, gas flow rate=56 mL min^{-1}, liquid flow rate=20 mL min^{-1}

Table1. Specifications of hydrophobic SPG glass membrane contactor

Parameter	Value	Units
Thickness (δ)	0.2	mm
Inner diameter of membrane (d_i)	10	mm
Outer diameter of membrane (d_o)	10.4	mm
Shell hydraulic diameter (d_h)	9.6	mm
Tortuosity (τ_m)	3	
Porosity of membrane (ε_m)	0.57	-
Shell side area (S_G)	7.84E-3	m^2
Tube side area (S_L)	8.16E-3	m^2
Number of tubes	1	-
Active length (L)	0.260	m

Table 2a. Physical properties of [Bmim][TCM]

Property	Value	Units	Ref.
Density	$\rho_L = 1.24018 + (-6.51429 \times 10^{-4}\ T)$	g.cm^{-3}	(Zubeir et al., 2015)
Viscosity	$\mu_L = \exp\left(-1.639 + (\dfrac{594.522}{T - 178.409})\right)$	mPa.s	(Zubeir et al., 2015)
Henry constant	$H_{co2} = 1166.5\ exp\left(\dfrac{-1633}{T}\right)$	MPa	(Zubeir et al., 2015)

Table 2b. Physical properties of gases

Property	Value	Units	Ref.
Molar volume of CO$_2$	26.9	cm^3.mol^{-1}	(Fuller et al., 1966)
Molar volume of H$_2$	7.07	cm^{3}mol^{-1}	(Fuller et al., 1966)
Viscosity of gas mixture	$\mu_g = 10^{-6}.\dfrac{Z_2 F_p F_q}{\xi}$	Pa.s	(Lucas, 1980)
Diffusivity of CO$_2$ in gas phase	$D_{g,co2} = \dfrac{10^{-8}T^{1.75}\sqrt{\left[\frac{1}{M_{CO2}} + \frac{1}{M_{H2}}\right]}}{(0.01P)[(v_{co2})^{0.33} + (v_{H2})^{0.33}]^2}$	m^2.s^{-1}	(Fuller et al., 1966)
Diffusivity of CO$_2$ in liquid phase	$D_{l,co2} = 2.66 \times 10^{-8}\dfrac{1}{\mu_L^{0.66}\ v_{co2}^{0.129}}$	m^2.s^{-1}	(Morgan et al., 2005)

Table 3. Operational parameters and constraints used in simulations

Parameter	Description	
Temperature (T)	22 -80 ^{o}C	
Gas phase inlet pressure (P_g)	1-20 bar	
Liquid phase inlet pressure (P_l)	1-20 bar	
Feed gas composition of CO_2	45 % (by volume)	
Absorbent concentration(at 22 ^{o}C) (C_{IL})	4.570 mol.L^{-1}	
CO_2-loading in absorbent at inlet	Fresh solvent (0)	
Liquid flow rate (LFR)	20 ml.min^{-1}	
Gas flow rate (GFR)	56 ml.min^{-1}	

Table 4. Contributions of mass transfer resistances of gas, liquid and membrane phases to the overall mass transfer resistance

Phase	Contribution to overall resistance(%) non-wetted mode	Contribution to overall resistance(%) wetted mode
Gas	1.9	1.2
Membrane	0.02	34.4
Liquid	67.0	44.0
Transport in liquid phase	31.1	20.4